Investigating Fluidisation of Powder in the Supply Bins of Polymer Laser Sintering Machines Using Foundational 2D Numerical Modelling

Fredrick Mwania[1,*], Maina Maringa[2] and Jacobus van der Walt[1]

[1]*Department of Mechanical and Mechatronic Engineering Central University of Technology, 20 President Brand Street, Bloemfontein, South Africa*

[2]*Department of Mechanical Engineering, Murang'a University of Technology, P. O. Box 75-10200 Murang'a, Kenya*

Abstract: Fluidisation is a critical process in polymer laser sintering, but limited studies have been conducted in this area. In this regard, two-dimensional numerical models were used, in this study, to establish a suitable flowrate and period of fluidization for a polypropylene powder material used as a feedstock in polymer laser sintering. The study also investigated the impact of different spreading parameters and properties of material such as, bulk-density, particle-size, and fluidised bed height, on the fluidisation behaviour of powder in the supply bins of EOS P380, P385, and P396 machines. A computational fluid dynamic (CFD) software, Fluent, was identified and applied to investigate the fluidisation behaviour of a polypropylene material. The results arising from the numerical modelling revealed that the suitable fluidisation-flowrate for the material considered is 20 liters/min and the period lies between one and three seconds. It was also established that it might be difficult to fluidise polymeric materials with a density equal to or greater than 1500 kg/m^3, particle sizes equal to or greater than 90 μm, and for bed heights below 0.10 m.

Keywords: Fluidisation-flowrate, fluidisation-time, bulk density, particle size, powder bed height.

1. INTRODUCTION

The use of numerical models to investigate the process of Powder Bed Fusion (PBF) for polymers (Polymer Laser Sintering) has gained considerable attention in the recent past. The technique provides useful and insightful information on Polymer Laser Sintering (PLS), which is not easily obtained through experimental methods [1]. However, most of the available studies mainly focus on the laser exposure and post-processing phases of the process, disregarding the pre-processes, such as powder-fluidisation in the powder supply bins. There is a need to develop numerical models to investigate fluidisation of powder in the supply bins of PLS machines because it affects the deposition of powder. Fluidisation of powder is pertinent because it ensures that the amount of powder deposited into the hopper of the double blade recoater unit is sufficient to form a single layer, for a specified layer thickness when spread on the platform in the build chamber (the depth by which the platform in the build chamber moves downwards).

According to Bopape [2], fluidised beds have high heat transfer coefficients and ensure that solid particles move like a fluid. Khawaja [3] added that fluidised beds provide uniform distribution of heat and ensure excellent mixing. In PLS, fluidisation also affects spreadability of powder, which influences the properties of finished parts. Loose powder causes cavities and defects to form in printed parts [4]. Moreover, powder-bed irregularities arising from difficulties of spreading fluidised powder improperly, affect the input of energy during the sintering phase, leading to poor part-quality in terms of mechanical strength[5, 6]. Le *et al*. [7] added that uniformity of the layer thickness and powder packing density determined the quality and performance of the final components. These issues can be addressed through proper fluidisation of the powder in the supply bins before being spread on the platform in the build chamber of a PLS machine. Therefore, it is imperative to investigate the fluidisation behaviour of powder under different conditions and for powders with different properties.

Fluidisation of a granular material is influenced by different factors such as flowrate of a fluid being introduced into a fluidisation bed, size of particles, and density of particles [3]. Farshi [8] stated that the minimum flowrate of fluidisation and bed-height are crucial hydrodynamic parameters that affected the level of fluidisation of a fluidised powder bed. Guevara [9] alluded that the impacts of height of the powder bed were negligible, whereas the fluidisation-flowrate and density of powder played a primary role on the behaviour of fluidised powder beds. The same view was supported by Sobrino *et al*. [10], who suggested that the minimum fluidisation flowrate is not significantly influenced by the changes in a settled depth of a powder bed.

Apart from the flowrate of the fluidising medium and size of particles, the density of particles also plays a key role in the fluidisation process [9]. Geldart [11]

*Address correspondence to this author at the Department of Mechanical and Mechatronic Engineering Central University of Technology, 20 President Brand Street, Bloemfontein, South Africa; Tel: +27 603599632;
E-mail: fredmulinge@gmail.com

classified granular materials into groups A, B, C, and D. Geldart group A has particles of sizes from 20 to 100 μm and a density of approximately 1400 kg/m^3. Such materials expand by a factor of 2 to 3 during fluidisation before initiation of bubbling, probably because they do not promote formation of large bubbles due to their relatively small size [12]. It is also expected that Geldart group A materials will exhibit easy, smooth, and homogenous fluidisation because as was stated by Bodhanwalla& Ramachandran [13], particles of small size (30 – 150 μm) and low density (1400kg/m^3) are easy to fluidise. Geldart group B materials consist of particles between sizes 40 and 500 μm, with densities between 1400 and 4500kg/m^3. Bubbling of Geldart group B materials commences at the start of fluidisation probably because the large particles encourage formation of large bubbles [12]. Geldart group C has particle sizes ranging from 20 to 30 μm, and are considered highly fine and cohesive materials, making them difficult to fluidise. Hence, they might require additional agitation to attain fluidisation. Lastly, Geldart group D has particle diameters above 600 μm and are considered to be materials with a broad density range [14]. They have high permeability, which results in severe bubbling and channelling. Their fluidisation can only be obtained at extremely high flowrates of the fluidisation medium. According to Sagar & Elangovan [15], suitable sizes of particles for polymeric materials used in PLS should be between 20 to 80μm. Therefore, most PLS materials can be considered to be Geldart group A-materials.

Polymer laser sintering is a sophisticated multi-factorial process drawing considerable attention from the academic and industrial communities. Recently, scientists have ventured into analytical and numerical modelling to provide more insights into the unknown details of PLS, such as fluidisation of powder. Numerical models can offer useful information on fluidisation of PLS polymeric powders to close the research gap on it. Gupta *et al*. [16] alluded that experimental investigation of the fluidisation process is complex and expensive. The authors further indicated that it was experimentally challenging to evaluate the essential process-details of a fluidisation process.

Polymeric powders in the supply bins are fluidised to promote deposition and spreadability. These are essential pre-processing steps of PLS that ensure that enough powder is spread uniformly across the platform in the build chamber of a PLS machine. Currently, operators utilise trial and error experimental methods to establish suitable fluidisation velocity for new materials, which is time consuming and tiresome. The current study was undertaken to develop numerical models using an ANSYS Fluent package to establish a suitable flowrate of fluidisation and fluidisation period for a commercial polypropylene material. The study also investigated the fluidisation behaviour of powder when different values of bulk density of the particles, size of the particles, and height of the fluidisation bed were considered. Numerical simulation, undertaken in this study, can be used to offer better insights into fluidisation of powder in PLS. Morever, the numerical models proposed in this work should help minimise the challenges and expenses associated with experimental techniques, especially when determining suitable fluidsation-flowrates for new feedstock materials.

2. AN OVERVIEW OF NUMERICAL MODELLING TECHNIQUES USED FOR INVESTIGATING FLUIDISATION OF POWDER

Khawaja [3] provided an overview of numerical modelling techniques used for prediction of the fluidisation of particles of powder. According to the author, interaction between two phases is commonly considered and can be modelled using Eulerian and Lagrangian methods. The former technique considers particles as a continuum and develops their equations of conservation on the basis of a control volume in a form similar to that of fluids, whereas the latter treats particles as a discrete phase and thus evaluates their trajectories separately. Furthermore, the discrete particles considered in the Lagrangian model are taken to obey Newton's law, whereas the Eulerian type of model is governed by the Navier-Stokes equations [17]. Van der Hoef *et al*. [17] and Al-Akaishi *et al*. [18] further described different models from these two primary models as outlined in Table **1**.

Both the solid and gas phases are considered as particles in the Lagrangian-Lagrangian (LL) molecular dynamics model, where the solid-gas interaction is represented by collisions. This model is suitable for systems at extremely small scales, where changes in temperature affect the motion of the particles. The Eulerian- Eulerian model (two-fluid) considers the two phases (solid and gas) as a continuum. The interaction of the two phases, in the Eulerian- Eulerian model, involves drag force correlations, which are subject to the velocities of the phases and the volume fraction of the solid phase. The model is common because of its affordable computational cost [16]. However, this model does not adequately evaluate particle-particle and particle-gas interactions. A comprehensive particle-gas interaction can be described using Discrete Particle Models (DPMs) that can be classified as either unresolved or resolved models. The Unresolved Discrete Particle Model (UDPM) is also referred to as Discrete Element Model and considers larger Eulerian grid compared to the particles. The gas-solid interaction is similar to that of the Eulerian-

Table 1: Different Models that can be Utilised to Describe a Gas-Solid System using Gas-Fluidisation

#	Type of Model	Model for the gas phase	Model for the solid phase	Gas-solid coupling	Application/scale
1	Discrete bubble model	Lagrangian	Eulerian	Drag closures for bubbles	Industrial (10m)
2	Two-fluid model	Eulerian	Eulerian	Gas-solid drag closures	Engineering (1m)
3	Unresolved discrete particle model	Eulerian (unresolved)	Lagrangian	Gas-particle drag closures	Laboratory (0.1m)
4	Resolved discrete particle model	Eulerian (resolved)	Lagrangian	Boundary condition at particle surface	Laboratory (0.01m)
5	Molecular dynamics	Lagrangian	Lagrangian	Elastic collisions at particle surface	Mesoscopic (<0.001m)

Eulerian model. The Resolved Discrete Particle Model (RDPM) is also known as Direct Numerical Simulation. In this model, the Eulerian grid is smaller than the particles, and allows computation of flow between the particles. It does not require correlations and gas-particle interaction are represented by a stick boundary condition on the surface of the particles. This model allows simulation of particle-particle and particle-gas interactions in a more realistic manner. Lastly, the Discrete Bubble Model considers the generated bubbles as discrete entities that can undergo collision, fusion, shrinkage, expansion, and disintegration.

3. PREVIOUS STUDIES ON THE INFLUENCE OF DIFFERENT FACTORS ON FLUIDISATION OF POWDER OF PARTICLES

Halvorsen & Arvoh [19] investigated the hydrodynamic properties (minimum velocity of fluidisation, the behaviour of bubbles, and drop of pressure) of fluidised beds with differing size ranges of particles using experimental and computational analysis. The authors used a laboratory-scale powder bed with width, depth, and height of 0.20 m, 0.025 m, and 0.80 m, respectively. Changes of pressure were measured at five different position on the powder bed, and a digital camera employed to record and observe the formation of bubbles and segregation of particles. The diameters of particles considered in this study are summarised in Table **2**.

Halvorsen & Arvoh [19] performed simulations using the mean diameters, and similar velocities and bed heights were considered as used for the experiments. A two-dimensional geometry was used and meshed using a grid size of 0.5 x 0.5 mm in the horizontal and vertical directions. The authors compared the behaviour of bubble formation for different combination of particle sizes using simulation and experimental setups. They started by using the smallest particles with a mean size diameter of 153 *μm* and a superficial velocity of 0.1 *m/s*. The simulations considered a one particle phase. Both the computational and experimental results revealed formation of a considerable number of large bubbles. In the second experiment, the researchers examined a mixture of 50% small and 50% medium particles with a mean diameter of 320 *μm*, where a superficial velocity of 0.1 *m/s* was considered. The simulation was conducted using two particle phases. The experimental results revealed a clear segregation of the particles, and formation of bubbles above the layer of large particles. The formation of the bubbles was also revealed by the computational results. However, the size of the bubbles was visibly smaller than in the first case. The third analysis involved using a mixture of 50% small and 50% large particles with a mean particle diameter of about 556 *μm*, and a superficial velocity of 0.1 *m/s*. The simulations were conducted using two particle phases of diameters 153 and 960 *μm*. Segregation of the particles was clearly observed in both the computational and experimental results. A fewer number of bubbles were visible compared to the first and second investigation. The authors then ran experiments and simulations using medium and large particles with superficial velocity of 0.20 *m/*s and 0.33 *m/s*, respectively. The experiments showed formation of relatively fewer bubbles compared to the other three previous analyses. However, the simulations showed fixed beds with no bubbles. The variations between the experimental and computational results, especially for the last investigation might have been due to constraints introduced in the simulations, such as using a single particle phase with the same mean size diameter. Overall, the study concluded that the formation of bubbles and size of the bubbles is inversely proportional to the size of particles, as shown in Figure **1**.

Al-Akaishi *et al*. [18] investigated hydrodynamic behaviour (porosity and instantaneous superficial velocity) of a gas-solid powder bed with different perforated distribution plates. The authors used the Discrete Phase Model (DPM) together with a Multiphase Particle-in-Cell (MPPIC) strategy to investigate a (800 mm height x 83 mm diameter) gasifier bed. The study indicated that the porosity of the

Table 2: The Diameters of Particles Considered in this Analysis

Experiment No.	Size-Range of Particles(μm)	Mean Diameter of Particles (μm)
1	100-200	153
2	400-600	488
3	750-1000	960
4	(100-200) & (400-600)	320
5	(100-200) & (750-1000)	556
6	(400-600) & (750-1000)	724

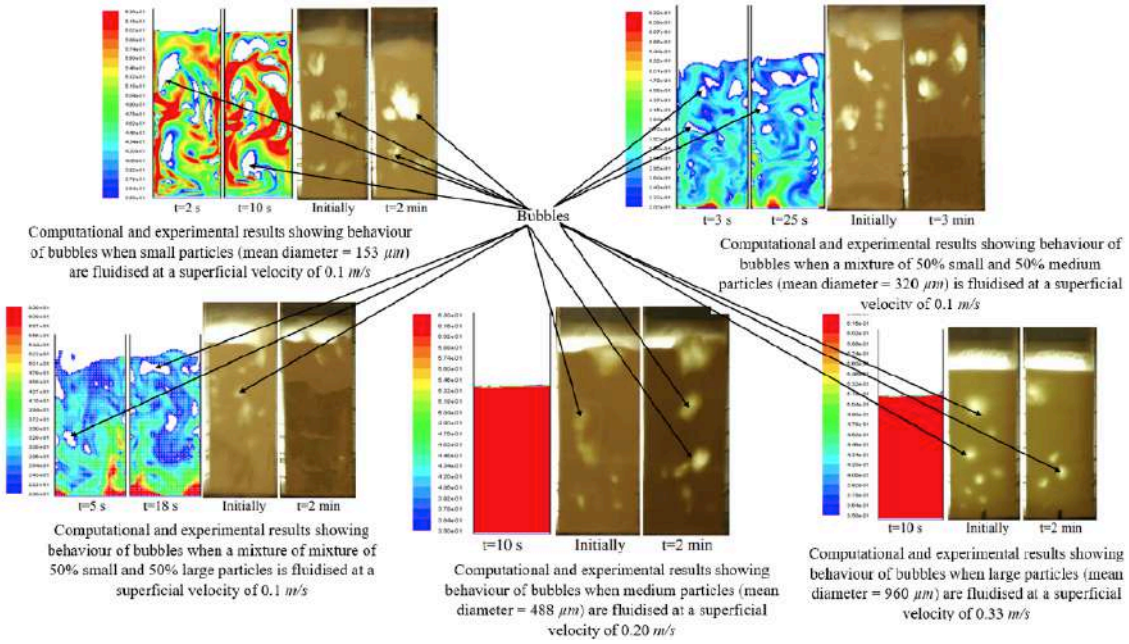

Figure 1: Influence of mean particle diameter on formation of bubbles and size of the bubbles during fluidisation (Experimental and computation comparison) [19].

gasifier bed increased with increasing superficial velocity, as shown by size and intensity of bubbles. The degree of porosity can be used as a measure for the density of particles, as well as the formation and size of bubbles in the fluidised bed.

De Vos [20] investigated the influence of morphology of particles on their entrainment, removal or carry over from the fluidised bed. The authors used a 140 mm Perspex column to fluidise spherical smooth-surfaced and irregular rough-surfaced ferrosilicon (FeSi) particles with the same solid density and average diameter (38-50 μm). The analysis revealed that spherical and smooth-surfaced particles exhibited high entrainment (six times) compared to the irregular particles with rough surfaces. In summary, the study showed that both the shape and surface finish of particles were some of the factors that influenced the quality of fluidisation of solid-gas powder beds.

Bandara *et al*. [21] investigated the impact of density, size, and distribution of particles on the minimum velocity of fluidisation for a fluidised powder bed. The authors employed the multiphase particle-in-cell method to assess the Eulerian-Lagrangian model using a commercial Barracuda VR package. The outcomes of the study indicated that the minimum velocity of fluidisation increased with increasing size and density of the particles. The effects of particle size distribution (PSD) were not well defined, but the analysis revealed that monodispersed particles exhibited the highest values of minimum velocity of fluidisation.

Fang *et al*. [22] modelled the minimum velocity of fluidisation and pressure-drop of a conical fluidised powder bed. In this work, the authors investigated the impact of varying size and mass of particles on the minimum velocity of fluidisation and pressure-drop of a fluidised powder bed. The outcomes of the study revealed that the minimum velocity of fluidisation increased with increasing size of particles but was not significantly influenced by the mass of the particles. To the contrary, the drop of pressure was found to be primarily influenced by the mass of the powders as opposed to the size of the particles.

Liao [23] investigated the effects of the shape of particles and height of the fluidised powder bed on the minimum velocity of fluidisation of a fluidised bed. The

authors stated that content of voids in a material on a fluidised powder bed increased with decreasing sphericity. Contrarily, the content of voids in a material on the fluidised powder bed decreased with increasing density of the particles and increasing height of the fluidised powder bed. Moreover, fluidisation decreased with decreasing minimum velocity of fluidisation velocity. Overall, the minimum velocity of fluidisation reduced with increasing density of the particles and increasing height of the fluidised powder bed and increased with decreasing sphericity.

Potgieter *et al*. [24] used a Eulerian-Eulerian granular model to simulate flow of a gas-solid fluidised bed. The authors developed numerical models usingCFD that revealed that no visible bubbles were observed in a fixed bed regime. Moreover, before attaining a minimum velocity of fluidisation, the pressure-drops increased while the height of the fluidisation powder bed remained constant. To the contrary, after fluidisation, the height of the fluidised powder bed increased whereas the pressure drop seemed to remain constant. Furthermore, the sizes of bubbles increased with increasing chamber height and increasing superficial velocity.

Xu & Yu [25] modelled a gas-solid fluidised bed using a combined approach of the discrete particle method and computational fluid dynamics (DPM-CFD). The author investigated the relationship between the pressure-drop in the fluidisation powder bed and superficial gas velocity using 2400 particles with a density of 2700 kgm^{-3} and average diameter of $4x10^{-3}$ m. A fluidised bed with dimensions of (length × width × height) $0.9 \times 0.15 \times 0.004$ m was considered in this study. The analysis revealed that the pressure-drop in the fluidisation powder bed increased (A-G) and then decreased (G-B) with increasing superficial gas velocity as illustrated in Figure **2**.

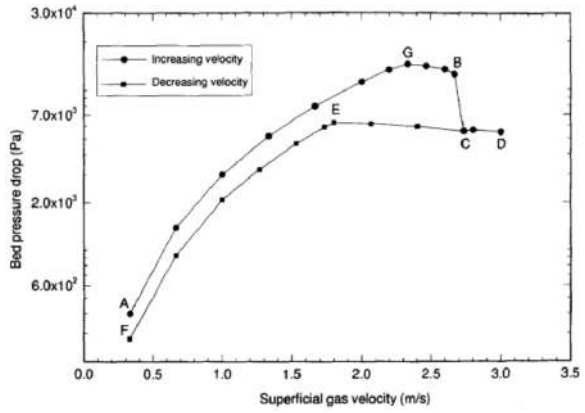

Figure 2: Relationship between fluidised powder bed pressure drop and superficial gas velocity during fluidisation [25].

The diagram illustrates different stages of fluidisation: point A-B to C (fixed bed stage), point C to D (fully fluidised bed stage), point C to E (incipient of fluidisation - the point at which fluidisation starts), and point E to F (de-fluidisation stage, which is the point at which a fluidisation powder bed starts to become unstable).

Abdulrahman *et al.* [26] performed experimental investigations and CFD simulation to analyse the hydrodynamic properties of liquid-solid fluidised beds. The authors assessed the effect of the superficial liquid velocity and solid particle diameter on minimum velocity of fluidisation, pressure drop, expansion of the fluidised powder bed, and individual phase holdup (volumetric fraction occupied by individual phases in a multiphase system). The particles of glass bead in this work had varying average diameters (0.003 m, 0.004 m, and 0.006 m) and a density of 2500 kg/m^3. A Perspex column with an internal diameter of 0.115 m and height of 1.7 m was used in the study. The pressure drop was measured using Keller type PA 21Y/4 differential pressure transducers. The study revealed that the drop of pressure in the powder increased continuously with increasing superficial water velocity until the powder bed became fluidised, then it remained constant. In addition, the value of pressure drop in the fluidisation powder bed and the minimum velocity of fluidisation increased with the increasing diameter of the glass beads. The authors also found that the fluidisation powder bed remained static until the minimum velocity of fluidisation was attained, after which, the expansion ratio (*R*) of the fluidised powder bed started to increase with increasing velocity of the liquid (water) as illustrated in Figure **3**. The expansion ratio of the fluidised powder bed was calculated as a quotient of height of the fluidised bed to its static height.

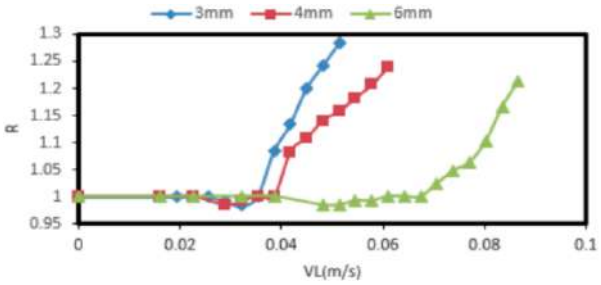

Figure 3: The relationship between the expansion ratio (*R*) of the fluidised powder bed with the increasing velocity of water [26].

Minimum velocity of fluidisation can also be determined using the solid or liquid holdup, which is the volume fraction occupied by the different phases in the system. Abdulrahman *et al*. [26] proposed Equations 1 and 2 for calculating solid and liquid holdup.

$$\varepsilon_S + \varepsilon_L = 1 \quad (1)$$

$$\varepsilon_S = \frac{M_S}{\rho_S A_S H_e} \quad (2)$$

where,

ε_S = solid holdup (fraction of solid phase)

ε_L = liquid holdup (fraction of the liquid phase)

M_s = mass of the solid contained in a column (*kg*)

ρ_s = density of the solid (kg/m^3)

A_s = cross-sectional area of the column (m^2)

H_e = expanded bed height (*m*)

Abdulrahman *et al*. [26] found that solid and liquid holdups remained static until the minimum velocity of fluidisation was reached. After this, the solid holdup started to decrease, while the liquid holdup increased, with increasing superficial velocity, as illustrate in Figures **4** and **5**.

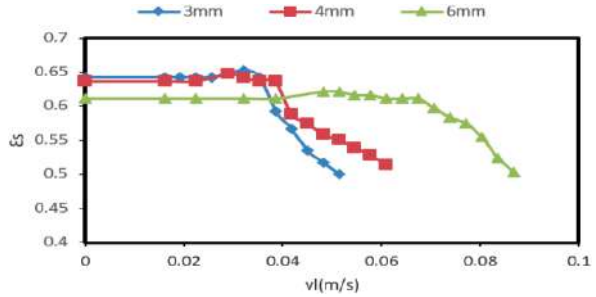

Figure 4: Relationship between solid holdup and superficial velocity of the fluid [26].

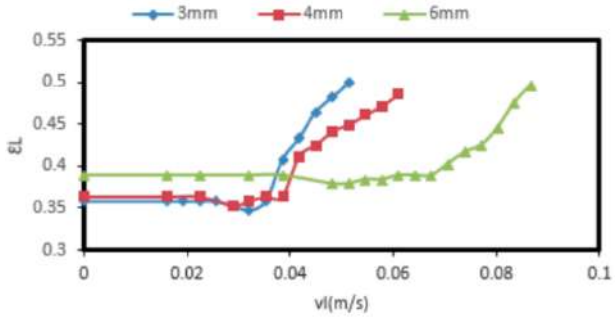

Figure 5: Relationship between liquid holdup and superficial velocity of the fluid [26].

Various research undertakings have investigated the influence of different factors on the fluidisation process, as illustrated from the foregoing literature review. However, these studies were not directed towards a particular application such as PLS. In this regard, the current research provides a novel and useful investigation offluidisation with a specific focus on PLS.

4. METHODOLOGY

4.1. The Process Being Modelled

The process modelled here is the fluidisation of polymeric powders in the supply bins of EOSINT P380, P385, and P396 machines. It is essential to determine suitable flowrates to ensure that the normally cohesive polymeric powders can be deposited in the correct quantities in the hopper of arecoater. Currently, most technicians employ trial and error approaches or consider values provided by suppliers of feedstock materials to set the flowrate of the stream of air used for fluidisation of powder. Hence, the need for a systematic approach to determine a suitable fluidisation flowrate required for each specific powder based on the cohesiveness, density, size, and shape distribution of its particles.

4.2. Models Considered in the Numerical Modelling

Numerical models are required to understand the flow characteristics of powder inside the supply bins to gain knowledge of powder fluidisation. In this regard, computational modelling was undertaken in this work. The choice was made to undertake modelling for a two-dimensional (2D) fluidised bed instead of a three-dimensional (3D) fluidised bed, for ease of evaluation and computation. The authors acknowledge limitations posed by 2D numerical modelling, such reduced accuracy of predicting gas-solid interactions. However, a foundational 2D study still offers crucial information, and forms a starting point for a 3D numerical analysis. Moreover, using 2D simulations is sufficient for studying hydrodynamic behavior (porosity, bed expansion) of fluidised beds, which is the fundamental concern for this analysis.

A student version of computational fluid dynamics (CFD) Fluent was used in this evaluation. A combination of the different model parameters outlined in Table **3**, were considered to define the phases and phase interaction. The models (outlined in Table **3**) were selected since they have been commonly employed to simulate fluidisation of powder bed as noted from a read of past papers [18, 19, 21, 22, 23, 24, 26]. The Eulerian model were considered because they save on computational time and are easy to model.

The standard Fluent models considered here (Syamlal-Obrien, Lun-et-al, Algebraic) do not account for cohesion forces, which are common for fine powders, especially if they are less than 30μm in size. This might affect the accuracy of the obtained results because PLS powders are considered cohesive. Decisively, this assumption was taken since the fluidisation forces are expected to overcome the cohesive forces, and the powder particles are supposed to behaviourlike free-flowing phase after fluidisation. This is also the reason Syamlal-Obrien model was favoured over other models (Gidaspow, Wen & Yu) to represent the drag model because it handles high-velocity gradients better.

Table 3: Model Parameters Used in Ansys Fluent

Property	Model
Gas phase	Eulerian
Solid phase	Eulerian
Drag coefficient	Syamlal-Obrien
Lift coefficient	None
Turbulent dispersion	None
Turbulence interaction	None
Radial distribution	Lun-et-al
Population balance model	Turned off
Granular viscosity	Syamlal-Obrien
Pressure of the solids	Lun-et-al
Granular temperature	Algebraic
Virtual mass coefficient	None
Surface tension coefficient	None

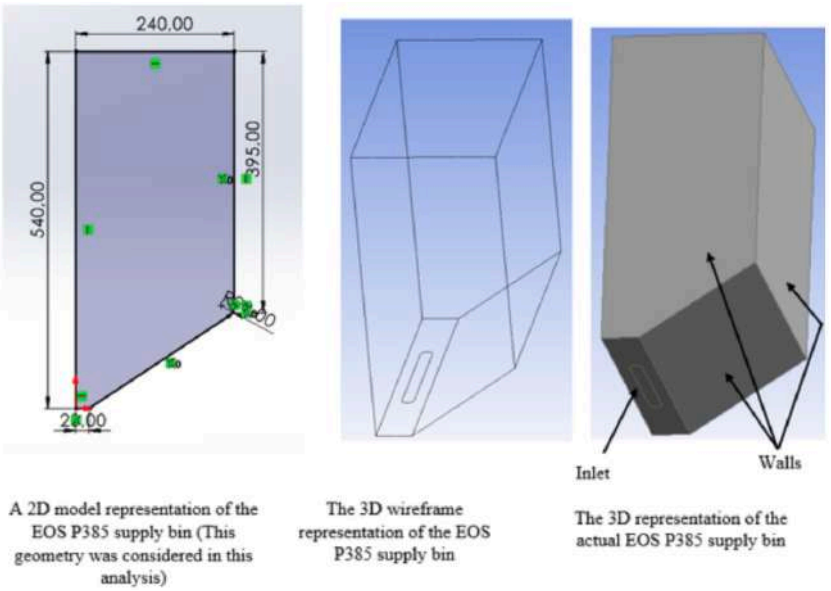

Figure 6: Two-dimensional and 3D representation of supply bin for EOS P385 machine.

4.3. Set Up of Simulation

4.3.1. Geometry

The geometry considered in this analysis is represented in Figure **6**. Actual dimensions were considered in the simulations. A two-dimensional (2D) cross-section, three-dimensional (3D) wireframe, and 3D solid representation of the supply bin for an EOS P385 machine are illustrated in Figure **6**. The dimensions are in millimetres.

The 2D geometry was adopted for the reasons given in the preceding paragraph and a student version Fluid Flow (Fluent) package used for analysis. The solver comprised of five steps: developing a geometry, meshing, setting up the model (setup), solution, and results, as illustrated in Figure **7**.

A 2D model of the supply bin was developed using Ansys Fluid Flow (Fluent) – Design Modeller (Figure **8**). The model can also be developed using other CAD software, such as SolidWorks and then be imported into Ansys Fluid Flow (Fluent).

4.3.2 Meshing

The geometry was meshed using the face meshing tool shown in Figure **9**. Other parameters of the mesh are summarisedin Table **4**. Lastly, different parts of the geometry (inlet, outlet, walls, and fluid-domain) were named as provided inFigure **10**.

4.3.2.1. Mesh Sensitivity Analysis

The reliability of computational investigations is a major concern in the scientific community because the accuracy of any findings is subject to the

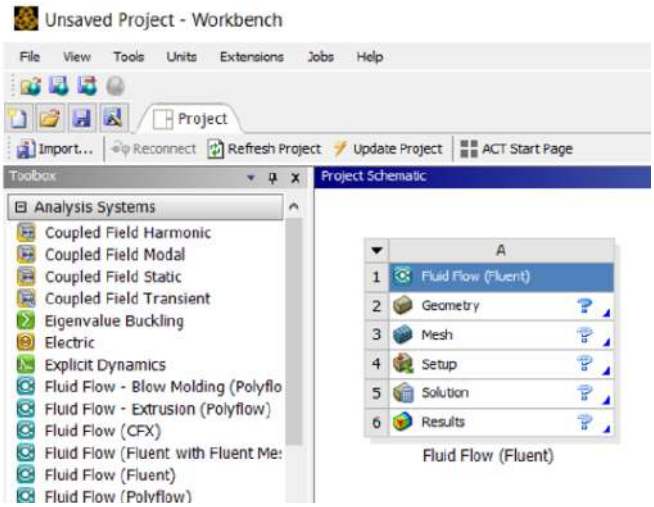

Figure 7: Fluid Flow (Fluent) setup of the solver.

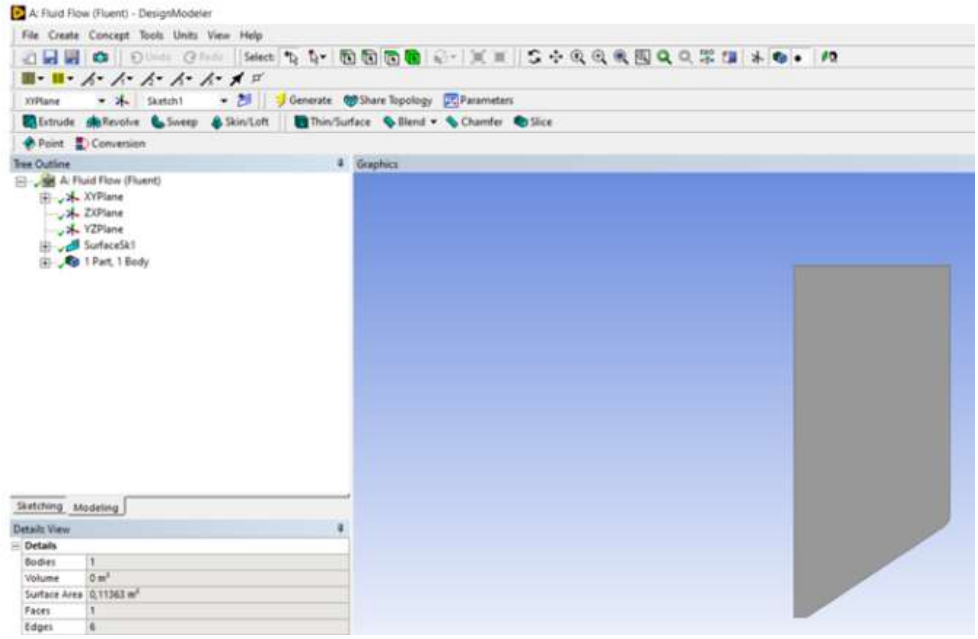

Figure 8: A 2D model of the supply bin developed using Ansys Fluid Flow (Fluent).

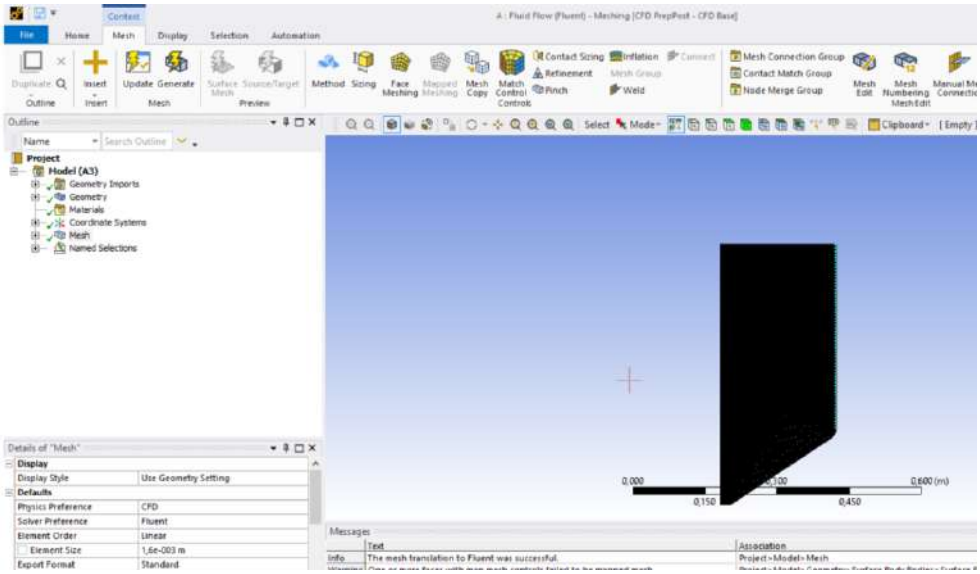

Figure 9: Meshing of the 2D model representing a planar view of a powder supply bin.

Table 4: Parameters of the Mesh used in this Analysis

#	Meshing Parameter	Value
1	Type of meshing	Face meshing
2	Element type	Linear (selected because of the simplicity of the geometry considered in this analysis)
3	Element size	0.0016 m (1.6 mm) (selected after a convergence test was undertaken)
4	Nodes	44982
5	Elements	44537

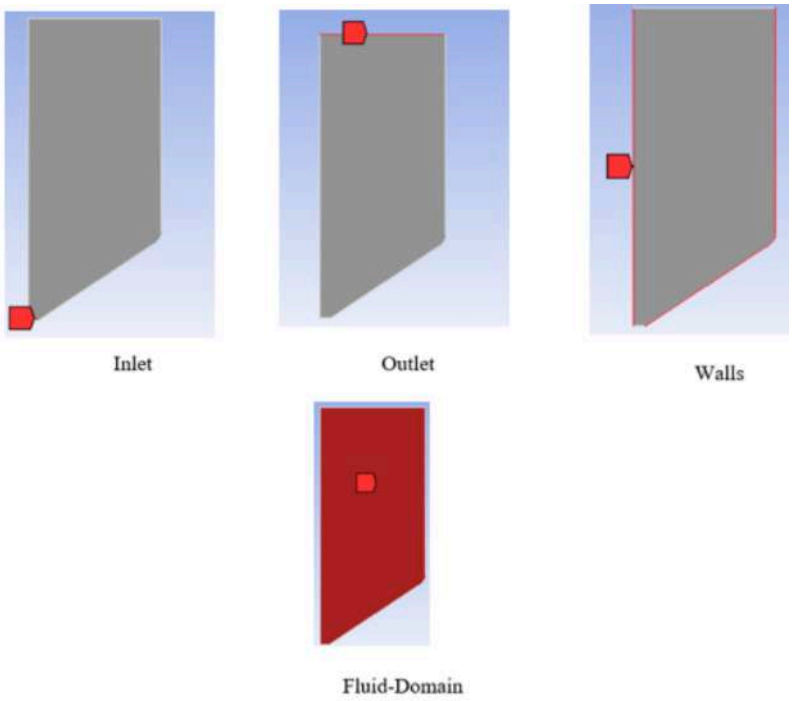

Figure 10: Different parts of a 2D supply bin geometry (inlet, outlet, walls, and fluid-domain).

characteristics of the mesh used. For instance, a study of mesh sensitivity is crucial since it ensures that solutions obtained from a computational analysis are independent from the resolution of the mesh [27]. This process is also referred to as mesh independence or mesh convergence study. Timsina and Barahmand [27] stated that different strategies can be employed for mesh independence tests. Some of the common techniques include general Richardson extrapolation, Grid Convergence Index (GCI), and grid resolution.

According to Timsina and Barahmand [27], the Richardson's extrapolation uses numerical analysis to predict the error in a solution by considering two different grid sizes. The error of the solution based on the Richardson's extrapolation can be determined using Equation3, which is a continuous and differentiable function [28].

$$E_h = f_{exact} - f_h = C_1 h + C_2 h^2 + C_3 h^3 + \cdots \quad (3)$$

where,

$E_h =$ error of a numerical solution

f = dependent variable

h = grid size

C = coefficient that can be a function of the coordinates, but not *h*. The value of *C* can be determined using Equation 4.

$$C = (f_{ext} - f_1)/h^n \quad (4)$$

n = apparent order of the method

The GCI method predicts grid discretization errors, allowing quantification of possible uncertainties [27]. The strategy considers a grid convergence error estimator that is based on the generalised Richardson Extrapolation methodology. Hence, a coarse and a fine grid is used to develop Equations 5 and 6, which describe the GCI for the fine grid and the grid discretization error [28].

$$GCI\ [fine\ grid] = F_s \frac{|\varepsilon|}{r^p - 1} \quad (5)$$

$$\varepsilon = \frac{f_2 - f_1}{f_1} \quad (6)$$

where,

F_s =factor of safety of the method

r = grid refinement ration (h_2/h_1) ($h_2$and $h_1$course and fine grid sizes)

p = order of accuracy of the numerical solution

f_i(i = 1, 2) = grid refinement factors (the relation between grid sizes h/h_1, h/h_2) and the simulated values respectively corresponding to the h_i grid size

The grid resolution technique involves gradually increasing the mesh size until the performance improvement cannot be observed [27]. The current study involved investigation of the behaviour of the powder material when subjected to air flow to determine the most suitable mesh size. Moreover, the total time for meshing and running simulations were considered in the analysis. Table **5** summarises the different mesh size considered, and it also outlines the number of nodes and elements for each case. The cross-sectional views of different grids are represented in Figure **11** (side views). The meshing was carried out using Dell Latitude E6430, Core i5 computer with a RAM capacity of 4 GB, 64-bit operating system, and processor speed of 2.70 Hz.

The mesh size, 0.5 mm, was disregarded because it took a significant time to complete the meshing process. After one hour, meshing was not complete when a mesh size of 0.5 mm was considered. This can be taken as a relatively long time, considering that a simple geometry and linear meshing pattern was employed in this case. After this, simulations involving the remaining mesh sizes (5.0, 3.0, 2.5, 2.0, 1.5, 1.0, 0.9, 0.8, 0.7, and 0.6 mm) were undertaken to determine the mesh size where the performance improvement could be observed despite reducing the mesh size. Figure **12** represents the results obtained from the mesh convergence test.

Figure **12** shows that the stability of the simulations was subject to the mesh size used. The results illustrate that the dispersion of the particles appears to be unstable when run for the mesh of the sizes 5.0, 3.0, and 2.5 mm. The impact of air flow through the powder

Table 5: The Mesh Sizes Considered during the mesh Sensitivity Analysis

#	Mesh size (mm)	Number of nodes	Number of elements	Time to mesh	Time to run 200 iterations	Total time mesh the model and to run the iterations
1	5.0	4732	4588	1 minute	3 minutes	4 minutes
2	3.0	12896	12656	1 minute	5 minutes	6 minutes
3	2.5	18520	18234	1 minute	6 minutes	7 minutes
4	2.0	28847	28490	1 minute	8 minutes	9 minutes
5	1.5	51083	50608	3 minutes	14 minutes	17 minutes
6	1.0	114517	113807	8 minutes	16 minutes	24 minutes
7	0.9	139740	138956	9 minutes	An Error	-

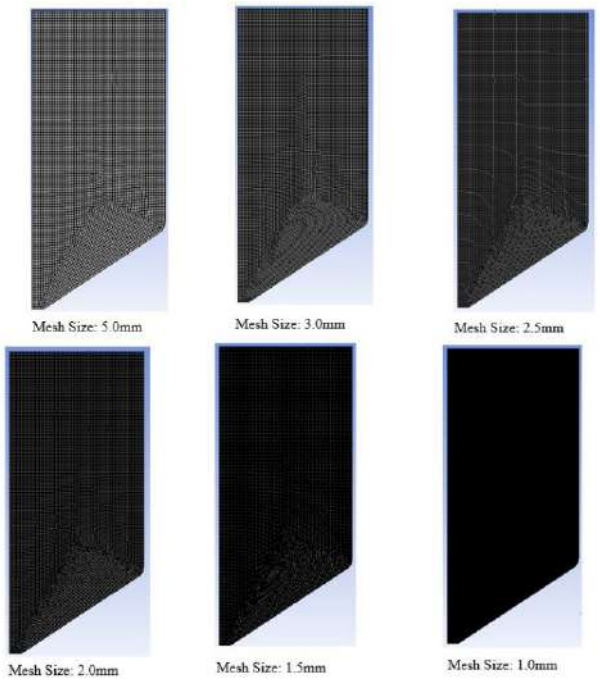

Figure 11: The cross-sectional views of different grids.

material in the supply bin is not visible for these mesh sizes. However, the behaviour of the particles when air is allowed to flow through the powder seems to stabilise for mesh sizes below 2 mm. The effects (formations of bubbles) of air flow through the powder were visible when mesh sizes of 1.5 and 1.0 mm were considered. An error was returned when a simulation was run for a mesh size of 0.9 mm. Hence, the mesh sizes at and below this value were disregarded. Hence, it was concluded that any mesh size between 1.0 and 1.5 mm could be utilised to study fluidisation of powder in the supply bins.

4.3.3. Setup of the Model

The model set-up followed determination of the appropriate mesh density and meshing, where double precision and 4 solvers were considered as illustrated in Figure **13**.Four solvers were selected because the license used is a student version.

For the general set-up, a pressure-based solver-type was selected and velocity formation set at absolute values. Steady time and 2D planar space were selected. Lastly, an acceleration due to gravity of 9.81 m/s^2 was selected for the Y-plane direction, as summarised in Figure **14**. A negative value of the gravitational acceleration was selected to prevent particles from leaving the domain with the flow.

The energy model under the model-module was then enabled. After this, the multi-phase model was enabled, where two Eulerian phases were selected as indicated in Figure **15**.

The materials were then added under the material-module. The fluid considered in this analysis was air, which had the properties detailed in Table **6**.

The particles considered here were polypropylene, and their specified properties are provided in Table **7**.

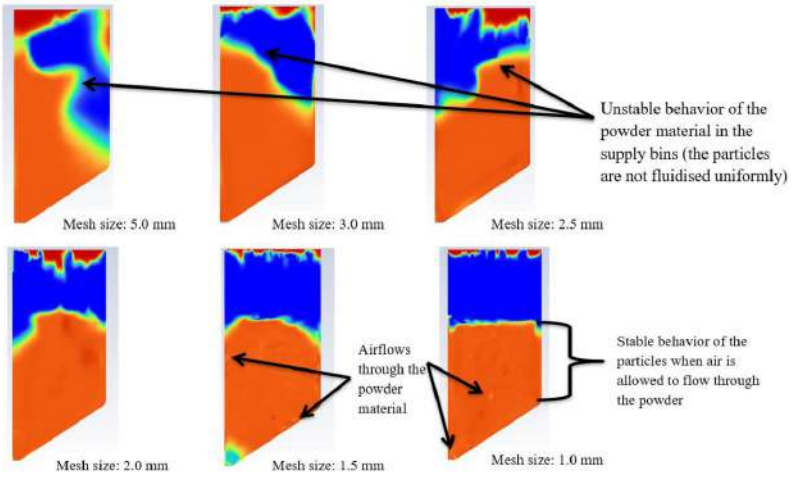

Figure 12: Results obtained from the mesh convergence test.

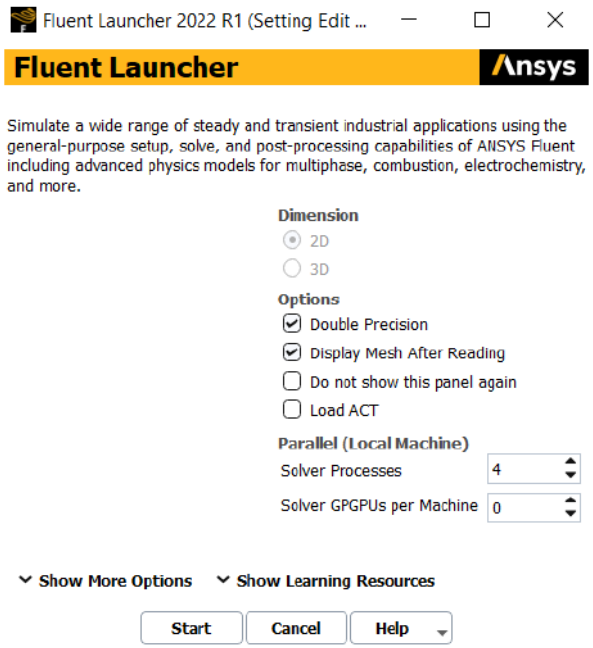

Figure 13: Launching the Fluid Flow (Fluent) solver.

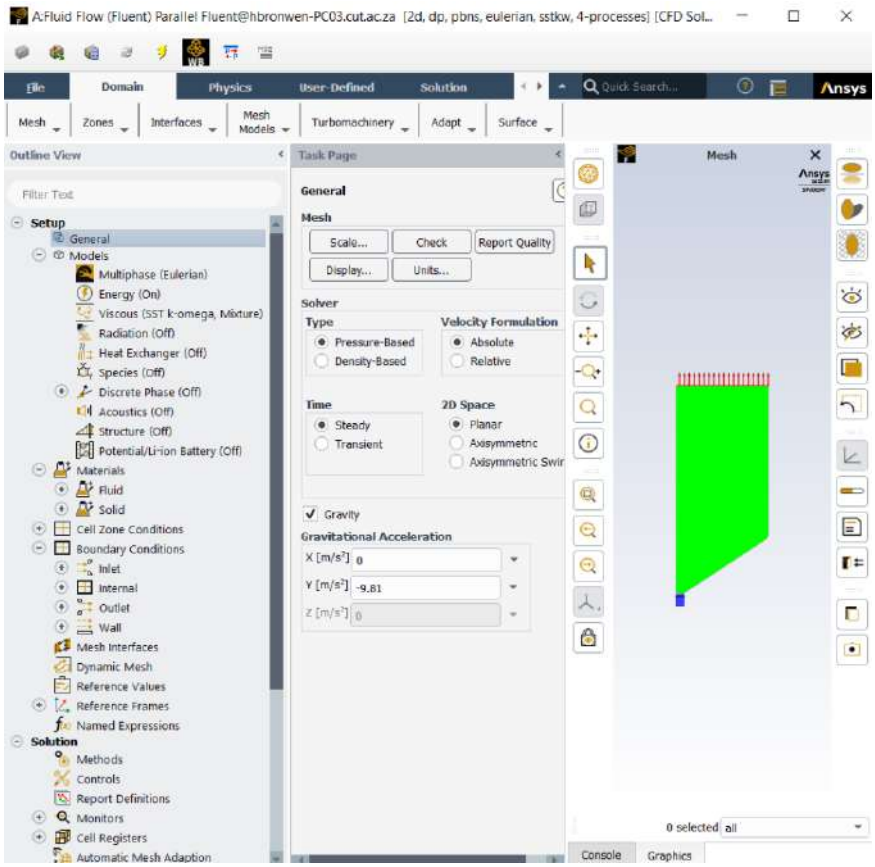

Figure 14: General set-up.

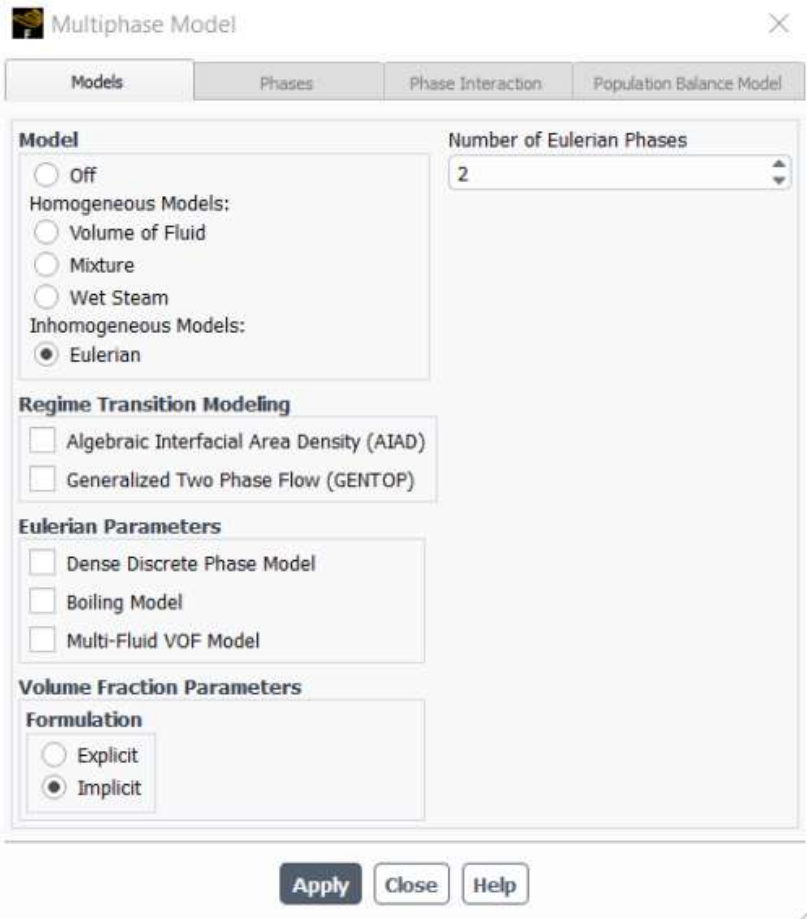

Figure 15: The multi-phase model set-up.

Table 6: Properties of the Fluid (air) used in this Analysis

#	Property	Value
1	Density	1.204 (kg/m^3)
2	Specific heat	1006.43 [J/(kg K)]
3	Thermal conductivity	0.0242 [W/(m K)]
4	Viscosity	7.5* 10^{-8} [kg/(m s)]
5	Molecular weight	28.966 (kg/kmol)
6	Reference temperature	298.15 K

Table 7: Properties of Polypropylene (Diapow PP MF) Particles in the Current Analysis

#	Property	Value
1	Particle type	Geldart A particles
2	Diameter	65 μm
3	Packing limit	0.75
4	Granular viscosity	Syamlal-Obrien
5	Bulk density	330 (kg/m^3)
6	Specific heat	1700 [J/(kg K)]
7	Thermal conductivity	0.22 [W/(m K)]
8	Granular bulk viscosity	7.5 × 10^{-8}[kg/(m s)]
9	Molecular weight	42.08 g.mol^{-1}
10	Reference temperature	298.15 K
11	Coefficient of restitution	0.9

The particles considered here were polypropylene, The thermal conductivity of polypropylene was calculated as an average of the different values presented by Patti & Acierno [29] from several studies. The specific heat for polypropylene was obtained from a scientific online website [30]. The values are the same as the ones provided by the supplier (Diamond Plastics, GmbH). Once the models, properties of the phases, and phase interaction models were defined, then the boundary conditions at the inlet, outlet, and fluid domain were defined. Lastly, the model was run and simulated using 200 iterations adopted here to reduce the time required to run the simulations, while ensuring the veracity of the results obtained. The analysis determined the most suitable fluidisation flowrate for Diapow PP MF powder. They were also used to investigate how changes in fluidisation time, material density, fluidisation flowrate, particle size, and bed depth (quantity of the material in the supply bins) influence the fluidisation of powder.

5. RESULTS AND DISCUSSION

5.1. Determining Suitable Fluidisation Flowrate for the Commercial Polypropylene Powder Considered in this Study

A suitable fluidisation flowrate for Diapow PP MF powder was determined using the numerical models developed here by changing the inlet flowrate of the fluidising gas (Table **8**) and observing the level of fluidisation and bubbling (Figure **16**). In this analysis, fluidisation-time, bulk-density, particle-size, and bed-depth, and packing-limit, were set at 2 s, 330 kg/m^3, 65 μm, 0.4m, and 0.8, respectively. Taorat *et al*. [31] recommended a packing value of 0.63, since it provides accurate steady state results for gas-solid fluidised bed models. The values for fluidisation-time, bed-depth, and packing-limit given here were selected because they provided clear images of the interaction between the particles of powder and air, thus allowing easy description of the impact of different parameters on fluidisation. This was in contrast to the images obtained when a packing value of 0.63 was considered. The bulk-density and particle-size are properties of the powder (Diapow PP MF) considered in this study.

The values of inlet velocity in (m^3/s) were converted to (*m/s*) by dividing them by the cross-sectional area of the inlet. The software makes used use superficial velocity (*m/s*), whereas the PLS machines utilises flowrate (*litre/min*).

Figure **16** represents the numerical models simulated using different inlet fluid velocities. An inspection of the obtained results illustrated that better homogeneity and stability of the powder was attained

Table 8: Inlet Velocities used to Establish the Suitable Fluidisation Velocity of a Commercial Polypropylene Powder

Trial 1	Inlet flowrate(litre/min)	Inlet flowrate (m^3/s)	Inlet superficial velocity(m/s)
1	5	8.3×10^{-5}	0.0026
2	10	1.7×10^{-4}	0.0052
3	15	0.00025	0.0070
4	20	0.00033	0.0102
5	25	0.00042	0.0130

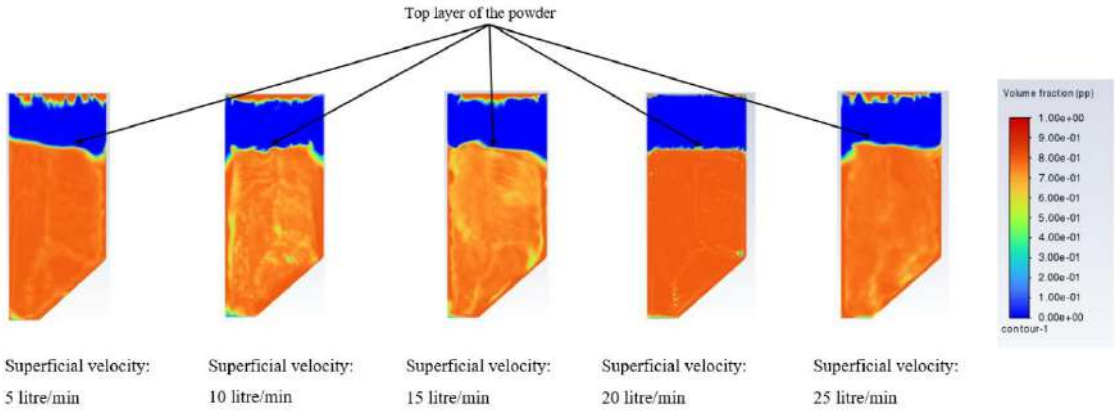

Figure 16: Fluidisation for different superficial inlet fluid velocities.

using an inlet velocity of 20 litre/min. The degree of homogeneity of powder is measured on the basis of the bubble-intensity (air pathways) in the powder bed. Stability was established based on the levelness of the top layer of the powder.

ImajeJ software was used to measure the level of bubble intensity using the 'mean gray value' command. This value determines the brightness of a pixel. It is expected that high numbers of 'mean gray value' indicate high bubble intensity, in this case, which translates to poorly fluidised beds.ImageJ software was employed for the other analysis involving time of fluidisation, density of powder, size of particles, and bed height.

A study by Al-Akaishi *et al*. [18] showed that air pathways and bubbling of a fluidised powder bed increased with the inlet flowrate. However, the results represented in Figure **16** indicate that an optimal flowrate exists, where the powder in the supply bin appears uniform and homogenous. In this study, the optimal flowrate was attained at 20 *litre/min*. This finding were confirmed by the 'mean gray values' represented by Figure **17** and Table **9**, where the lowest value was observed at 20 *litre/min*, an indication of a desirable fluidisation.

A significant standard deviation was observed, which is an indication that flowrate of fluidisation has a considerable influence onfluidisation process as noted by Farshi [8] and Guevara [9].

5.2. A Matrix of Different Values of Fluidisation Time, Density of Powder, Size of Particles, and Depth of Fluidisation Bed Considered in this Study

An inlet flowrate of air of 20 litres/min was considered the most suitable flowrate for fluidising DiaPow PP MF powder from Diamond Plastics, GmbH because the fluidised bed appeared more stable, and a significant homogeneity of the particles of powder could be seen. This velocity was used to evaluate the impact of fluidisation-time, density of particles, size of particles, and depth of fluidisation bed, upon fluidisation of powder. All these factors are illustrated in Table **10**. The values of the bulk densities and particle sizes were selected based on the values of the existing commercial powders.

5.3. Investigating the Fluidisation behaviour of Powder when Different Values of Fluidisation-Times are Considered

Figure **18** represents simulations of fluidisation at different durations of fluidisation. An inlet flowrate, bulk-density, particle-size, and bed-depth of 20 litre/min, 330 kg/m^3, 65μm, and 0.4m, respectively, were used for this simulation. It was observed that bubbling started to form after the fourth second. This can be seen in Figure **19** and Table **11**, where there is a sudden jump of bubble intensity after the fourth second. The sizes of the bubbles were seen to increase (through visual inspection) with fluidisation time. Hence, based on this simulation the most suitable fluidisation

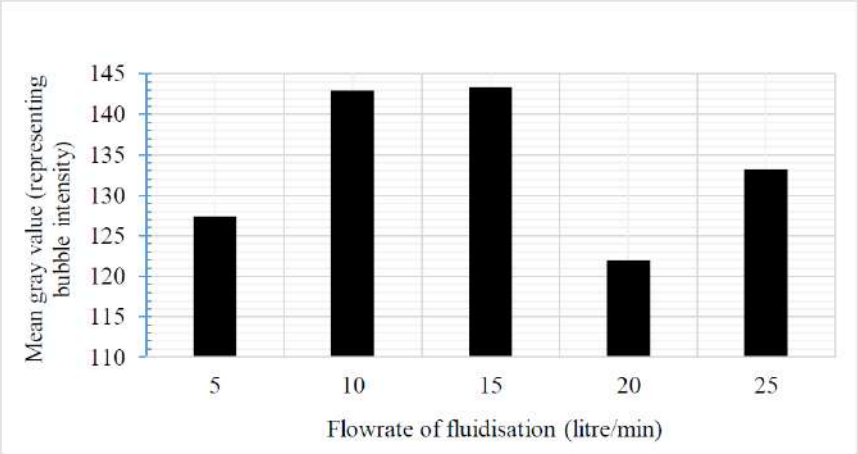

Figure 17: Bubble intensity for different flowrates of fluidisation.

Table 9: Bubble Intensity for Different Flowrates of Fluidisation

Flowrates of fluidisation(litre/min)	Mean gray value (representing bubble intensity)
5	127.407
10	142.979
15	143.375
20	121.922
25	133.157
Standard deviation	9.464

Table 10: Values Of Fluidisation-Time, Bulk Density of Powder, Size of Particles, and Depth of the Fluidisation Bed used Considered for this Analysis

Fluidisation time (s)	Bulk density (kg/m^3)	Particle size (μm)	Bed depth (m)
1	350	30	0.10
2	500	50	0.25
4	800	90	0.30
4	1000	100	0.35
10	1500	150	0.45

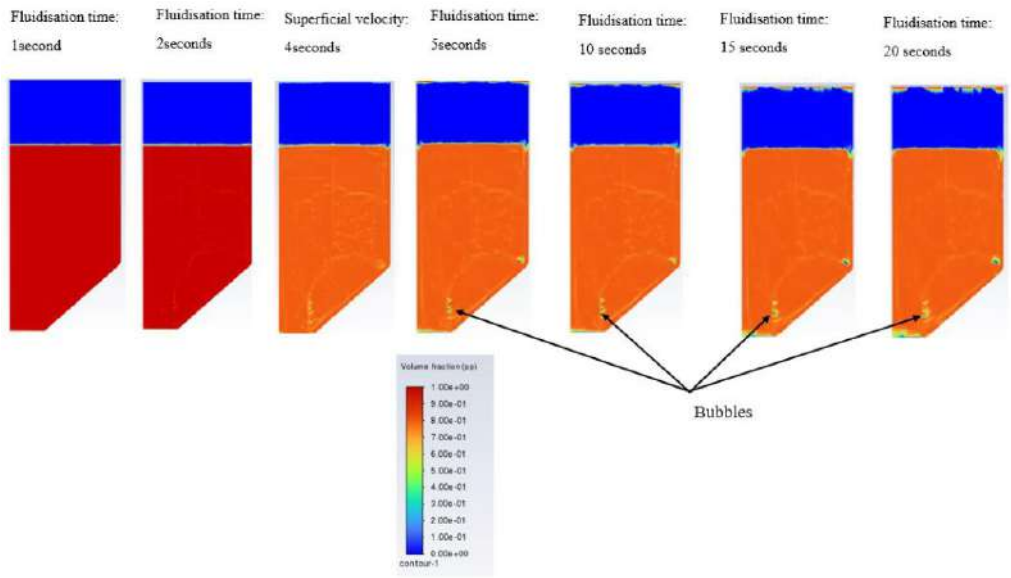

Figure 18: Simulations of fluidisation for different fluidisation times.

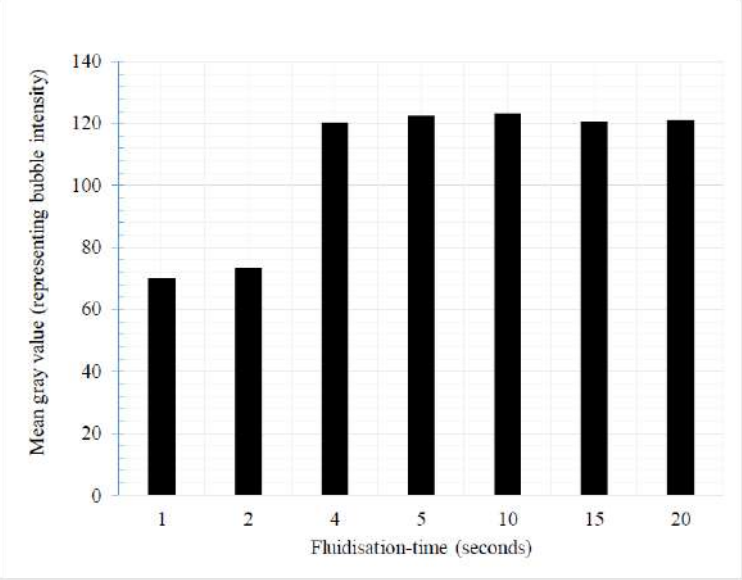

Figure 19: Bubble intensity for different durations of fluidisation.

Table 11: Bubble Intensity for Different Fluidisation-Times

Fluidisation-times (seconds)	Mean gray value (representing bubble intensity)
1	69.982
2	7.392
4	120.218
5	122.475
10	123.235
15	120.430
20	120.921
Standard deviation	24.328

time for Diapow PP MF powder from Diamond Plastics is suggested to be between one and three seconds. The standard deviation is quite considerable, which is evidence that fluidisation-time is extremely crucial and impactful during fluidisation of powder in PLS.

5.4. Investigating the Fluidisation behaviour of Powder when Different values of Powder Densities are Considered

Figure **20** represents the fluidisation simulations for powders with different bulk densities of materials. An inlet flowrate of 20 litre/min was considered, and all simulations run for 3 seconds. The particle-size and bed-depth were maintained at 65μm, and 0.4m, respectively. The powders with bulk densities of 300, 500, and 800 kg/m^3, did not show considerable difference in terms of bubble-intensity. However, a notable increase in bubble-intensity was visible for powder with a bulk density of 1000 kg/m^3. The bubble-intensity became even more pronounced for powder with a bulk density of 1500 kg/m^3, as it is seen in Figure **21** and Table **12**. A significant standard deviation was observed, indicating importance of bulk densities on fluidisation phenomenon.

It is important to remember here that the bubble intensity refers to the size and number of air ways through the powder. High bubble-intensity reduces the homogeneity of powder, which is undesirable for powders in PLS. Improperly fluidised powder results in a powder bed with cavities on the powder bed of a PLS machine after recoating. The results obtained here support the separate findings of Geldart [11] and Bodhanwalla & Ramachandran [13], which illustrated that Geldart group A powders with bulk material densities less than 1400 kg/m^3 are easier to fluidise. The two studies showed that Geldart group B materials, which have densities between 1400 and 4500 kg/m^3 exhibited large number of big-sized bubbles, a condition which is discouraged in PLS.

5.5. Investigating the Fluidisation behaviour of Powder for Different Values of Mean Diameters of Particles of Powder

Figure **22** illustrates the simulations of fluidisation when particles with varying sizes were used. An inlet fluid flowrate of 20 litre/min was considered, and the simulations run for 3 seconds. The bulk density and

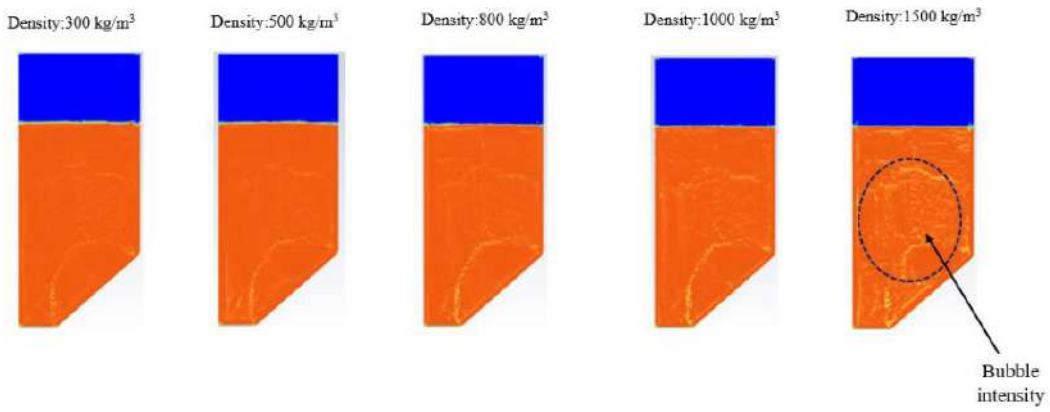

Figure 20: Simulations of fluidisation for different bulk densities (300 kg/m^3, 500 kg/m^3, 800 kg/m^3, 1000 kg/m^3, 1500 kg/m^3).

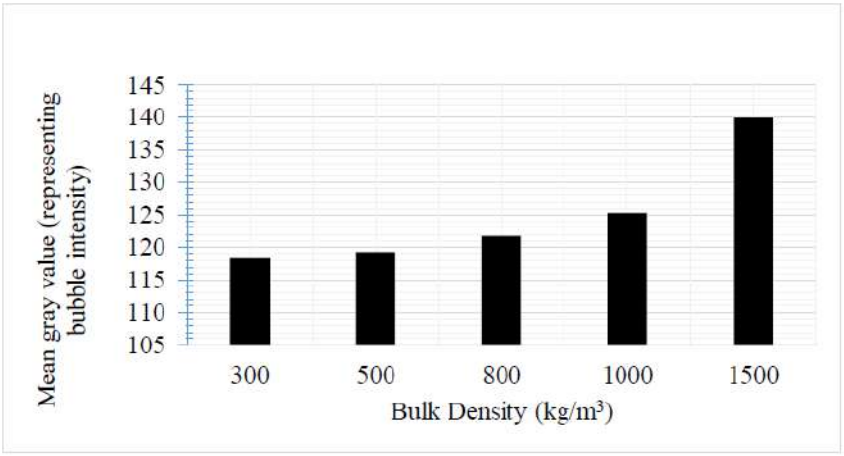

Figure 21: Bubble intensity for different bulk densities.

Table 12: Bubble Intensity for Different Bulk Densities

Bulk density (kg/m^3)	Mean gray value (representing bubble intensity)
300	118.418
500	119.250
800	121.756
1000	125.306
1500	139.870
Standard deviation	8.776

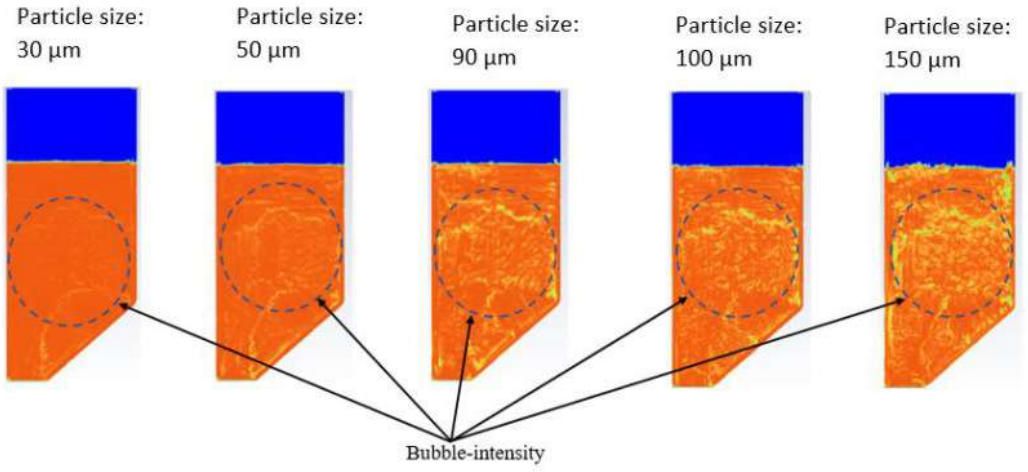

Figure 22: Simulations of fluidisation for different particle sizes (30 µm, 50 µm, 90 µm, 100 µm, and 150 µm).

bed-depth were maintained at 330 kg/m^3 and 0.4m, respectively. A small bubble-intensity was observed for the powder with particles of size 30 µm. The simulations in this set, indicate that bubble-intensity generally increased with increasing size of particles, as since in Figure **23** and Table **13**. Hence, it would become increasingly more difficult to attain a homogenous powder bed as the size of powder particles increased. The standard deviation illustrate that particle sizes affect fluidisation behaviour of powder, but not to the extend caused by fluidisation-time, flowrate of fluidisation, and bulk density.

Geldart [11] suggested that Geldart group C materials with particle sizes ranging from 20 to 30 µm would require additional agitation to attain fluidisation because they are highly cohesive. Geldart [11] added that Geldart group B materials, that have mean diameters between 40 and 500 µm, encourage formation of unwanted bubbling because of the large particles. Geldart group A, with particles of sizes from 20 to 100 µm was noted to be easier to fluidise, resulting into homogenous fluidisation. These findings are in agreement with the outcomes of the study by Abdulrahman *et al.* [26], which illustrated that it would be easier to fluidiseparticles of powder with small mean size diameters.

5.6. Investigating the Fluidisation behaviour of Powder for Different Bed Heights

Figure **24** illustrates simulations of fluidisation for different heights of the fluidisation bed. The inlet-flowrate, fluidisation-time, bulk-density, and mean particle-size were maintained at 20 litre/min, 3 s, 330 kg/m^3, and 0.4m, respectively. The highest bubble-intensity was seen to have occurred for the

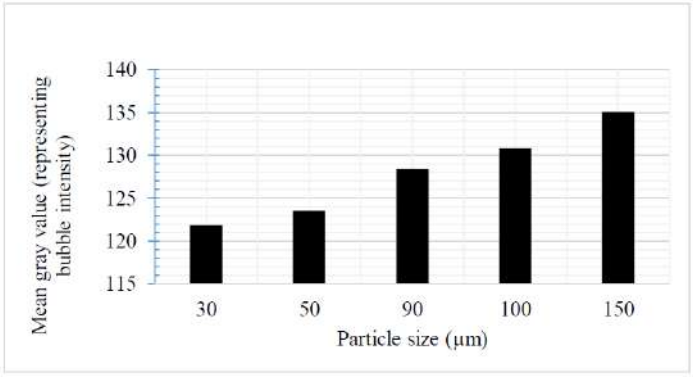

Figure 23: Bubble intensity for different particle sizes.

Table 13: Bubble Intensity for Different Particle Sizes

Particle sizes (µm)	Mean gray value (representing bubble intensity)
30	121.845
50	123.488
90	128.412
100	130.810
120	135.074
Standard deviation	5.342

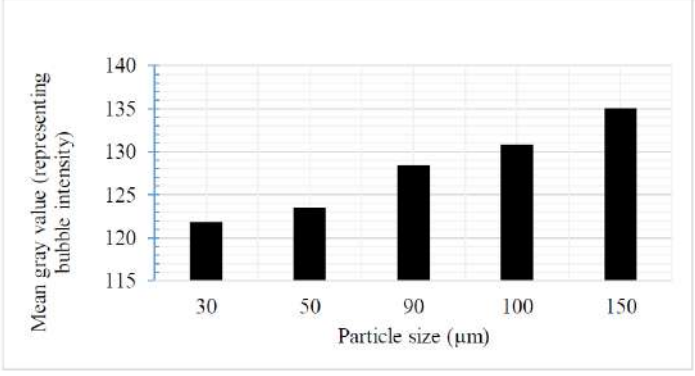

Figure 24: Simulations of fluidisation for different heights of the fluidisation bed of 0.1 m, 0.25 m, 0.30 m, 0.35 m, and 0.45 m.

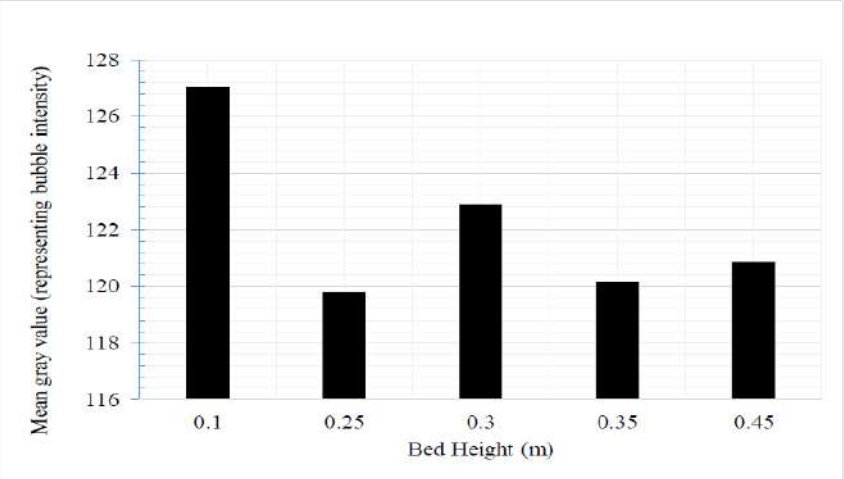

Figure 25: Bubble intensity for different bed heights of fluidised beds.

Table 14: Bubble Intensity for Different Bed Heights

Bed heights (m)	Mean gray value (representing bubble intensity)
0.10	127.039
0.25	119.792
0.30	122.912
0.35	120.148
0.45	120.864
Standard deviation	2.988

height of 0.10 m, and no particular trend was observed for the other bed heights (Figure **25**, Table **14**). This slightly differs with the findings by Liao [23] and Potgieter *et al*. [24], who observed that voids in a fluidised powder decreased with increasing fluidisation bed height. However, a significant drop in bubble intensity was seen beyond a bed height of 0.10m.The standard deviation value shown in Table **14** shows that bed height has minimal influence on the fluidisation of powder. This finding is in agreement with Guevara [9].

The results show that for asuitable fluidisation was achieved for bed heights more than 0.10 m. Hence, PLS demands use of large amounts of powder to ensure fluidisation for a supply bin of a fixed size. This can be challenging in research, since small amounts of feedstock are normally used to cut down on costs. The findings then demand design and production of smaller supply bins for research.

5.7. Implications for machine operation, design, and feedstock quality control

The findings from this analysis provide crucial information that inform on PLS machine operations, design, and feedstock quality control procedures. For instance, the best fluidisation time for Diapow PP MF powder was determined to be between one and three seconds. Hence, it is recommended that a timer relay be installed in EOSINT P385/P380/P395 machines or in future machines to regulate fluidisation time. The same concept has successfully been implemented at the Centre for Rapid Prototyping and Manufacturing (Central University of Technology, Free State), where relays have been used to regulate the fluidisation time. Moreover, the findings illustrate that it is not productive to attempt to fluidise polymeric materials with bulk densities equal to or greater than 1500 kg/m^3. Therefore, powder-manufacturers should aim to develop polymeric materials with densities below 1500 kg/m^3 considering the need for proper fluidisation. Manufacturers should also produce powders with particles with mean average sizeless than 90 µm, since the findings indicate that particles beyond this mean size are improperly fluidised. Machine operators should also ensure that the bed height remains higher that 0.10 m for successful fluidisation.

6. CONCLUSIONS AND RECOMMENDATIONS

The following conclusions and recommendations were derived from this analysis.

- ✓ A flowrate of fluidisation of 20 litres/min was the most suitable for fluidising Laser Diapow PP MF polypropylene powder.

- ✓ The best fluidisation period for the polypropylene powder considered in this study was determined to lie between one and three seconds.
- ✓ It would be unproductive to attempt fluidisation of polymeric materials with densities equal to or greater than 1500 kg/m^3.
- ✓ It would be relatively difficult to fluidise polymeric materials with particle of sizes equal to or greater than 90 μm.
- ✓ It would be easy to achieve a homogenous powder bed with fluidisation heights greater than 0.10 m as opposed to the case of a powder bed with heights below 0.10 m.
- ✓ The order of influence of different factors on fluidisation phenomenon,investigated here,in descending order (from the most impactful) is fluidisation-time, flowrate of fluidisation, bulk density, particle size, and bed height.
- ✓ This analysis focuses on a particular grade of polypropylene powder, and the findings might differ for other popular polymeric materials, such as polyamide (PA12), polyamide 11 (PA11), polyamide 6 (PA6), or thermoplastic polyurethane (TPU) due to differing material-properties. However, it provides pertinent information on thefluidisation phenomenon in PLS. The detailed procedure, provided in the study, can be employed for other polymers, especially for new materials, where few studies have been conducted. The procedure is also applicable for other machines with different bin geometries to that of EOSINT P385/P380/P395 machines.
- ✓ It is suggested that numerical models be developed using a 3D geometry to confirm the accuracy of the 2D models simulated here.

AUTHOR CONTRIBUTIONS

Conceptualization, FM.; methodology, FM; software, FM; validation, FM., MM. and JvdW; formal analysis, FM., MM. and JvdW; investigation, FM., MM. and JvdW; data curation, FM., MM. and JvdW; writing—original draft preparation, FM; writing—review and editing, FM., MM. and JvdW; visualization, FM.; supervision, MM. and JvdW.; project administration, MM. and JvdW; funding acquisition, MM. and JvdW.

FUNDING

South African Department of Science and Innovation Collaborative Program in Additive Manufacturing (Contract № CSIR-NLC-CPAM-21-MOA-CUT-03).

DATA AVAILABILITY STATEMENT

Data is available on request.

CONFLICT OF INTEREST

The authors declare no conflicts of interest.

REFERENCES

[1] Li J, Yuan S, Zhu J, Li S, Zhang W. Numerical model and experimental validation for laser sinterable semi-crystalline polymer: shrinkage and warping. Polymers 2020; 12(6): 1373-1411. https://doi.org/10.3390/polym12061373

[2] Bopape NF. CFD modelling of an ammonium nitrate fluidised bed: effect of distribution plate geometry. Doctoral dissertation, North-West University 2019.

[3] Khawaja HA. Review of the phenomenon of fluidisation and its numerical modelling techniques. The International Journal of Multiphysics 2015; 9(4): 397-407. https://doi.org/10.1260/1750-9548.9.4.397

[4] Lee Y, Simunovic S, Gurnon AK. Quantification of Powder Spreading Process for Metal Additive Manufacturing. ORNL/TM-2019/1382; CRADA/NFE-17-06812. Oak Ridge National Lab. (ORNL), Oak Ridge, TN (United States) 2019.

[5] Seita M. A high-resolution and large field-of-view scanner for in-line characterization of powder bed defects during additive manufacturing. Materials & Design 2019; 164(1): 107562-107571. https://doi.org/10.1016/j.matdes.2018.107562

[6] Zhang J, Tan Y, Bao T, Xu Y, Xiao X, Jiang S. Discrete element simulation of the effect of roller-spreading parameters on powder-bed density in additive manufacturing. Materials 2020; 13(10): 2285-2300. https://doi.org/10.3390/ma13102285

[7] Le TP, Wang X, Davidson KP, Fronda JE, Seita M. Experimental analysis of powder layer quality as a function of feedstock and recoating strategies. Additive Manufacturing 2021; 39(1): 101890-101914. https://doi.org/10.1016/j.addma.2021.101890

[8] Farshi A. Experimental measurement of different fluidisation parameters. Petroleum & Coal 2013; 55(4): 311-321.

[9] Farshi A. Experimental measurement of different fluidisation parameters. Petroleum & Coal 2013; 55(4): 311-321.

[10] Guevara DE. Bed Height and Material Density Effects on Fluidized Bed Hydrodynamics. Iowa State University (Thesis-Masters) 2010.

[11] Sobrino C, Almendros-Ibáñez JA, Santana D, De Vega M. Fluidisation of Group B particles with a rotating distributor. Powder Technology 2008; 181(3): 273-280. https://doi.org/10.1016/j.powtec.2007.05.014

[12] Geldart D. Types of gas fluidisation. Powder Technology 1973; 7(5): 285-292. https://doi.org/10.1016/0032-5910(73)80037-3

[13] Cocco R, Karri SR, Knowlton T. Introduction to fluidisation. Chem. Eng. Prog 2014; 110(11): 21-29.

[14] Bodhanwalla H, Ramachandran M. Parameters affecting the Fluidized bed performance: A review. REST Journal on Emerging Trends in Modelling and Manufacturing 2017; 3(1): 17-21.

[15] Rovero G, Curti M, Cavaglià G. Optimization of Spouted bed scale-up by square-based multiple unit design. Adv. Chem. Eng. 2012. https://doi.org/10.5772/33395

[16] Sagar MB, Elangovan K. Consolidation & factors influencing sintering process in polymer powder based additive

manufacturing. IOP Conference Series: Materials Science and Engineering 2017; 225(1): 1-9. https://doi.org/10.1088/1757-899X/225/1/012075

[17] Gupta S, Bhaskaran S, De S. Numerical modelling of fluidized bed gasification: An overview. Coal and biomass gasification 2018: 243-280. https://doi.org/10.1007/978-981-10-7335-9_10

[18] van der Hoef MA, van SintAnnaland M, Deen NG, Kuipers JAM. Numerical simulation of dense gas-solid fluidized beds: a multiscale modeling strategy. Annu. Rev. Fluid Mech. 2008; 40(1): 47-70. https://doi.org/10.1146/annurev.fluid.40.111406.102130

[19] Al-Akaishi A, Valera-Medina A, Chong CT, Marsh R. CFD analysis of the fluidised bed hydrodynamic behaviour inside an isothermal gasifier with different perforated plate distributors. Energy Procedia 2017; 142: 835-840. https://doi.org/10.1016/j.egypro.2017.12.134

[20] Halvorsen BM, Arvoh B. Minimum fluidisation velocity, bubble behaviour and pressure drop in fluidized beds with a range of particle sizes. WIT Transactions on Engineering Sciences 2009; 63(1): 227-238. https://doi.org/10.2495/MPF090201

[21] De Vos WP. The effect of particle shape on solid entrainment in gas-solid fluidisation. Masters dissertation, University of Pretoria 2008.

[22] Bandara J, Eikeland MS, Moldestad BME. Analyzing the effects of particle density, size, size distribution and shape for minimum fluidisation velocity with Eulerian-Lagrangian CFD simulation. Proceedings of the 58th SIMS, September 25th - 27th, Reykjavik, Iceland 2017.

[23] Fang S, Wei Y, Fu L, Tian G, Qu H. Modeling of the minimum fluidisation velocity and the incipient fluidisation pressure drop in a conical fluidized bed with negative pressure. Applied Sciences 2020; 10(24): 8764-8783. https://doi.org/10.3390/app10248764

[24] Liao L. Influence of particle shape and bed height on fluidisation. Masters dissertation, University of Florida 2013.

[25] Potgieter A, Bhamjee M, Kruger S. Modelling of a heated gas-solid fluidised bed using Eulerian based models. R&D Journal 2021; 37(6): 45-57. https://doi.org/10.17159/2309-8988/2021/v37a6

[26] Xu BH, Yu AB. Numerical simulation of the gas-solid flow in a fluidized bed by combining discrete particle method with computational fluid dynamics. Chemical Engineering Science 1997; 52(16): 2785-2809. https://doi.org/10.1016/S0009-2509(97)00081-X

[27] Abdulrahman AA, Mahdy OS, Sabri LS, Sultan AJ, Al-Naseri H, Hasan ZW, Ali JM. Experimental Investigation and Computational Fluid Dynamic Simulation of Hydrodynamics of Liquid–Solid Fluidized Beds. ChemEngineering 2022; 6(3): 37-55. https://doi.org/10.3390/chemengineering6030037

[28] Timsina R, Barahmand Z. Mesh Sensitivity Analysis of an Entrained Flow Biomass Gasifier: A CPFD Study. Scandinavian Simulation Society 2022; 63(1): 371-377. https://doi.org/10.3384/ecp192053

[29] Carrillo VM, Petrie JE, Pacheco EA. Application of the grid convergence index to a laminar axisymmetric sudden expansion flow. Maskana 2014; 5: 115-123.

[30] Patti A, Acierno D. Thermal conductivity of polypropylene-based materials. Polypropylene—Polymerization and Characterization of Mechanical and Thermal Properties 2020. https://doi.org/10.5772/intechopen.84477

[31] Nuclear Power for Everybody. Polypropylene-Density-Strength-Melting Point-Thermal conductivity. Retrieved from https://material-properties.org/polypropylene-density-strength-melting-point-thermal conductivity/#:~:text=Polypropylene%20%E2%80%93%20Specific%20Heat,is%201700%20J%2Fg%20K. (Accessed on 26/08/2022).

[32] Taorat K, Bumrungthaichaichan E, Wattananusorn S. Influence of Packing Limit on Gas-Solid Fluidized Bed Flow Pattern by Computational Fluid Dynamics. Ladkrabang Engineering Journal 2016; 33(1): 30-35.

Received on 22-12-2025 Accepted on 20-01-2026 Published on 18-02-2026

https://doi.org/10.6000/1929-5995.2026.15.04